Journal of Energy Storage 140 (2025) 119155

Contents lists available at ScienceDirect

Journal of Energy Storage

journal homepage: www.elsevier.com/locate/est

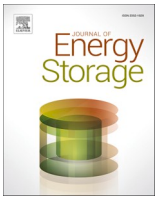

Research papers

Optimizing off-grid PV/wind systems with battery and water storage for rural energy and water access

Misagh Irandoostshahrestani *, Daniel R. Rousse

Industrial research group in Technologies of Energy and Energy Efficiency (t3e), École de Technologie Supérieure (ÉTS), University of Québec, Montréal, QC, H3C 1K3, Canada

ARTICLE INFO

Keywords:
Water pumping systems
Wind turbine
Loss of power supply probability
Water shortage probability
Multi- objective optimization
Solar energy

ABSTRACT

This study presents a multi-objective optimization framework for improving affordability, reliability, and water access in standalone off-grid energy systems integrating photovoltaic (PV) panels, wind turbines (WT), battery storage, and water reservoirs. The system is designed to meet both residential load demand and water needs. A mathematical model and a tailored Energy Management System (EMS) algorithm optimize power generation, energy storage, and water pumping. The EMS prioritizes residential electricity supply, ensuring battery charging for nighttime and low-irradiation periods, while excess power is used for water storage. Main performance parameters including Loss of Power Supply Probability (LPSP), Water Shortage Probability (WSP), and Capital Expenditure (CapEx) are optimized using a genetic algorithm (GA)-based multi-objective technique in order to enhance reliability, water availability, and cost efficiency of the system. A detailed financial model and reliability analysis evaluate system performance, with a case study in a remote island in Quebec demonstrating the feasibility of an autonomous, off-grid energy solution. The results show that the optimized system could effectively supply residential electricity while utilizing surplus power for water pumping—thus, reducing reliance on diesel generators (DG) or grid electricity. The proposed solutions showed a payback period of 8 to 12 years with LCOE in the range of 16.3 ¢/kWh to 23.4 ¢/kWh.

1. Introduction

Around 750 million people in the world have no access to electricity in 2023, and they are mostly located in sub-Saharan Africa [1]. Solar power systems are crucial in solving global warming, and to secure energy supply, and helping economic growth. Affordability, scalability, and environmental sustainability are the main factors that justify their extensive use [2].

Based on the importance of solar power systems, studies have investigated their use in water supply for off-grid communities. Meunier et al. [3] studied a PV water pumping system (PVWPS) designed to supply water for a rural, off-grid community in a village in Burkina Faso. The model was validated through experiments and it considered users' water consumption patterns and climatic data of ambient temperature and solar irradiance. The model calculates the discharge rate of the pump and water level in the water storage system. The study focused on the architecture of the PVWPS and the water tank and its control loop that determines the starting and stopping of the pumping system based on water height in the reservoir. The study also investigates a methodology for evaluating coefficients related to system performance. It was revealed that the proposed model can predict the water level and the discharge rate in different solar and weather conditions with good accuracy. The authors concluded that their model can be reliably applied in sub-Saharan Africa for performance evaluation and sizing of PVWPS projects.

In another study, Bakelli et al. [4] analyzed a PV water pumping system for supplying drinking water to remote villages in Ghardaia, Algeria. The study considered a daily water requirement of 6 cubic meters. The optimization model developed in the study employed the LPSP concept to evaluate the reliability of the system and the life cycle cost for economic assessment. The LPSP values was in the range of 0 % to 5 % that shows different levels of reliability. The model discusses the configurations of the system leading to these reliability values at the minimum life cycle cost while considering CapEx, replacement costs,

* Corresponding author.
E-mail address: misagh.irandoostshahrestani.1@ens.etsmtl.ca (M. Irandoostshahrestani).

https://doi.org/10.1016/j.est.2025.119155
Received 5 June 2025; Received in revised form 7 September 2025; Accepted 22 October 2025
Available online 28 October 2025

and operations and maintenance costs in the lifetime of the project. This study shows the effect of nominal power of PV modules and water storage tank size on reliability of the system and its cost. The life cycle cost analysis was done for pump heads of 6, 14, and 26 m at different LPSP values. The results showed that making a balance between PV panel numbers and water storage capacity is important for minimizing costs with regards to reliability parameters. For example, for LPSP of 0, the study showed that the optimal system configuration is different based on head and reliability criteria. This shows that it is necessity to evaluate each application individually based on the approach proposed in the study. This case study shows the importance of a comprehensive strategy to design and optimize a PVWPS and it also reveals the need for balancing reliability with economic parameters.

In another study by Bhayo et al. [5], a standalone PV-battery system for a water pumping application was investigated. The goal was to optimize power generation and utilization of surplus energy for a rural housing unit in Malaysia with a daily load requirement of 3.2 kWh. Utilizing real-time weather data and residential load requirements, the study developed an algorithm to lower the Levelized Cost of Energy (LCOE) while ensuring system reliability (LPSP = 0) and using the excess power for water pumping. The investigation evaluates the adaptability of the system to varying weather conditions, and shows its potential for rural electrification. By finding optimal PV and battery configurations, the importance of integrated renewable energy systems in finding economic and reliable energy solutions for rural communities is shown. The results revealed that the selected PV-battery system includes 2.44 kW_p PV system and 3.55 kWh battery backup capacity. This system could produce approximately 9.8 kWh of electricity and pump 363 cubic meters (m^3) of water daily.

In a multi-objective optimization study by Muhsen et al. [6], three parameters: life cycle cost, loss of load probability, and amount of excess water, were taken into consideration for a PVWPS designed to provide a constant daily water volume of 30 m^3 for the typical consumption of 120 people, based on meteorological data from Kuala Lumpur, Malaysia. A constant static head of 20 m was assumed for water pumping. A wide range of weighting factor sets was used to address the challenge of initializing weights for the objective functions. The study showed that the optimized configuration consisted of 20 PV modules and a maximum water reservoir capacity of 52 m^3, which resulted in a loss of load probability of approximately 0.5 % and achieving an average water flow rate of 3.3 m^3/h during pumping.

In recent study conducted by Irandoostshahrestani and Rousse [7], a techno-economic analysis was conducted on a small-scale PVWPS. The study focused on a farm in Bandar Abbas, a city located in the south of Iran. The system involves PV panels, batteries, inverters, and a water-pumping system. The research used the WSP and LPSP concepts for sizing of the system. The findings showed the considerable impact of LPSP and WSP values on both system size and cost. For example, LPSP increase from 0 to 3 % resulted to 55 % reduction in the LCOE and a decrease of about 36 % in WSP. In addition, it was shown that changing the PV panel nominal capacity can considerably affect the reliability of the system and its costs. Therefore, the paper concludes that it is essential to evaluate each project based on user requirements, including water access, power reliability and capital expenditures.

A recent study explored the use of hybrid photovoltaic/wind turbine (PV/WT) energy systems to provide affordable and reliable power. El-Maaroufi et al. [8] studied an off-grid PV/WT system with battery and hydrogen storage for Laayoune city, Morocco. They used HOMER Pro to find the best system design that reduces costs and improves reliability. Their results showed that a 100 % renewable energy system is possible without relying on fossil fuels. The optimized system produced steady electricity at a low cost of $0.0477/kWh. Furthermore, the study evaluated GHG emissions and concluded that integrating various energy sources with storage systems make the system reliable, economic, and sustainable.

In another research, Al-Omari et al. [9] conducted a feasibility study for a hybrid PV/WT system for electrifying a water pumping system in a village in Jordan, aiming to replace expensive and polluting conventional diesel generators. Here again, HOMER was used for the optimization of this off-grid system with the objectives of reducing environmental impact and cost and improving reliability. They showed that the hybrid system could achieve an LCOE of $0.241/kWh with a payback period of less than seven years, demonstrating that the system is feasible, and sustainable for a rural community.

A recent review by Irandoostshahrestani and Rousse [10] studied the current state of PVWPS in Iran, considering both technical aspects and broader socio-economic factors. Their study showed that PVWPS have been applied successfully in different climatic regions of the country, demonstrating good adaptability even in provinces with lower solar irradiation. The review discussed progress in areas such as panel cooling, tilt angle optimization, and control strategies, while also noting ongoing challenges including the high upfront investment cost, reliance on imported components, and the influence of fuel subsidies on economic competitiveness. The authors concluded that PVWPS can play an important role in reducing greenhouse gas emissions, improving irrigation reliability, and lowering long-term operating costs. However, they emphasized that wider adoption will depend on supportive policies, financial incentives, and design approaches suited to local conditions. These conclusions reinforce the need for integrated solutions that combine technical optimization with cost-effective and reliable performance.

Recent work continues to enrich the understanding of hybrid renewable systems through co-optimization of energy, water, and storage configurations. Shaier et al. [11] built a multi-objective framework that compares battery storage with supercapacitors and hydrogen storage to demonstrate how diverse storage technologies can jointly enhance system reliability while lowering cost. Wang et al. [12] examined a hybrid pumped-hydro–wind–PV system using the Normal Boundary Intersection method to simultaneously optimize channel utilization and minimize residual load fluctuations. Their findings highlight that carefully tuning the capacities of PV, wind, and pumped storage units improves operational flexibility and significantly boosts renewable utilization. Li et al. [13] deployed a wind–pumped storage hybrid system with scenario-based Pareto optimization to minimize levelized cost of energy, smooth net load, and reduce output deviation.

Despite the progress reported in the literature on PV-based water pumping systems and hybrid PV/WT systems for rural electrification, significant gaps remain. Most prior studies have either focused on single-resource systems (PV-only) or have optimized hybrid systems solely for electricity generation without explicitly considering water pumping as a co-primary objective. Furthermore, few studies have adopted a comprehensive multi-objective approach that simultaneously optimizes electricity reliability (LPSP), water access reliability (WSP), and capital expenditure (CapEx) while considering practical constraints such as land availability, seasonal resource variability, and realistic component lifespans. The present study addresses these gaps by developing a dual-application, fully renewable hybrid PV/WT-battery-reservoir system designed to meet both residential electricity and water demands in a remote community with no grid access. The work is motivated by the need to reduce reliance on costly and polluting diesel generators, to exploit the complementary nature of solar and wind resources to enhance year-round reliability, and to productively use surplus renewable energy for water pumping to increase community resilience. The novelty of this study lies in the development of a tailored energy management system that prioritizes electricity demand and uses excess power for water pumping, the application of a multi-objective genetic algorithm (NSGA-II) to jointly size PV arrays, wind turbines, battery banks, and water reservoirs under realistic constraints, and the use of a

real case study in Îles-de-la-Madeleine, Québec, to capture seasonal resource complementarity. In addition, a detailed techno-economic analysis including the levelized cost of energy and payback period is presented to demonstrate the feasibility and economic viability of achieving high renewable energy penetration in remote regions.

2. Schematic of the system and energy management algorithm

The system's schematic is illustrated in Fig. 1. The PV panels and the WTs generate the required electricity for the residents, and when the load demand is met, the excess power is used for battery charging. When the batteries are fully charged, the remaining excess power is directed to the pumping system, and the pumped water is stored in reservoirs.

The algorithm of the genuine methodology is shown in Fig. 2. As shown, the best tilt angle for maximum annual total irradiation is determined. Then, when the power load demand is met, the battery banks are charged and finally, the water pumping system is run when there is an excess power produced by the panels and the wind turbines, i.e., when the load demand is met, and the batteries are fully charged. The algorithm incorporates loops to calculate various PV, WT, and battery capacities together with appropriate water tank volumes. Finally, using the Non-dominated Sorting Genetic Algorithm II (NSGA-II), the optimized PV/ WT and battery bank nominal capacities and water storage tank volumes are selected based on minimized LPSP, WSP, and CapEx.

3. Case study

Îles-de-la-Madeleine, located in the Gulf of Saint Lawrence, Quebec, Canada, at a latitude of 47.40°N and a longitude of 61.77°W, was selected for this case study. Data from the NSRDB [14] for the most recent available year, i.e., 2023, was used. Fig. 3 shows the monthly average variations in GHI, ambient temperature, and albedo coefficient. As shown, the minimum monthly average temperature is −4.9 °C in February, while the maximum is 17.8 °C in July. The albedo coefficient is higher in winter because the ground is snow-covered. Furthermore, the monthly average of GHI ranges widely from 0.58 kWh/m^2-day in December to 5.96 kWh/m^2-day in July. In addition, windspeed variation throughout the year at hunheight is shown in Fig. 4.

There are several small communities in the Îles-de-la-Madeleine, the archipelago has a total population of about 13,000 people, spread across several villages and hamlets. Among these places, some are particularly small and isolated. For example, Grosse-Île is a unique English-speaking community in the region, with a relatively small population. Hence, in this case study, the water demand profile corresponds to a small community of 100 people, each with a constant daily water requirement of 260 L per person [15] resulting in a total daily demand of 26 m^3/day. This fixed demand was used to size the pumping system and reservoir storage in all simulations. The electricity consumption is obtained from the Canadian Centre for Energy Information database [16]. Since this data reflects the average of all electricity-consuming sectors, including residential, commercial, and industrial, it is scaled with respect to the annual consumption of households in Quebec, which equals 17,000 kWh/year [17], Fig. 5.

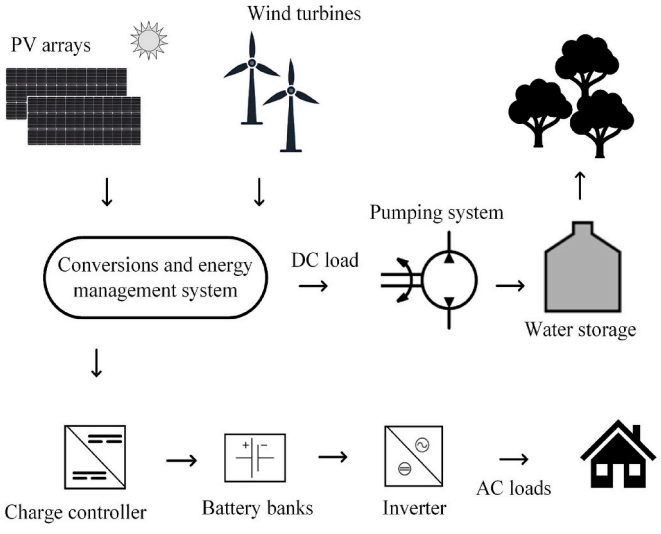

Fig. 1. Schematic of the system.

4. Methodology

In this section, the mathematical models are presented. Python is used to solve the mathematical model. Basic solar radiation models are provided in Appendix A. In the following sections, PV, WT, battery, water pumping and storage, reliability, and financial models, as well as the optimization procedure, are explained.

4.1. Solar PV system

To determine the power generated by the PV panels at each time step, the following equation is used [5,18,19]:

$$P_{PV}(t) = N_{PV} \times P_{PV,r} \times \left(\frac{G(t)}{G_{STC}}\right) \times \left[1 + \alpha \times \left(T_C(t) - T_{C,STC}\right)\right] \quad (1)$$

where N_{PV} is the total number of PV panels, $P_{PV,r}$ is the rated power of each panel under Standard Test Conditions (STC), G(t) is global solar radiation on the inclined surface at time t, G_{STC} is the solar irradiance under STC (equal to 1000 W/m^2), α is temperature coefficient of power (usually provided in the PV datasheet), $T_{C,STC}$ is cell temperature under STC (equal to 25 °C). The cell temperature at time t is calculated using the following equation [19]:

$$T_C(t) = T_{amb} + (NOCT - 20) \times \left(\frac{G(t)}{G_{NOCT}}\right) \quad (2)$$

where NOCT is the Nominal Operating Cell Temperature, which should be obtained from the PV datasheet, T_{amb} is the ambient temperature, and G_{NOCT} is the reference radiation at nominal conditions (equal to 800 W/m^2). Due to the area limitations for the PV panels, the maximum allowable PV panel number ($N_{PV,max}$) is set to 600:

$$1 \le N_{PV} \le N_{PV,max} \quad (3)$$

4.2. Wind turbine system

In this section, the output power of the wind turbine is described. The following equation is used to calculate the output power at standard temperature and pressure (STP) conditions [20,21] as described by [22]:

$$P_{WT,STP} = \begin{cases} 0, & V \le V_{c-in} \\ \dfrac{V^3 - V_{c-in}^3}{V_r^3 - V_{c-in}^3}, & V_{c-in} < V < V_r \\ P_r, & V_r \le V < V_{c-out} \\ 0, & V \ge V_{c-out} \end{cases} \quad (4)$$

where V_{c-in}, V_{c-out}, and V_r are the cut-in, cut-out, and rated windspeed. P_r is the rated power of the WT. The values of these parameters are given in Table 2 in Section 5. Specifications of the components. The wind speed at hub heigh should be obtained. As mentioned previously, wind speed data from NSRDB [14] were used, and the data is given for a height of 2 m. The following equation [23] is used to scale the windspeed to the WT's hub height:

$$V = V_{ref} \times \left(\frac{H}{H_{ref}}\right)^{\alpha} \quad (5)$$

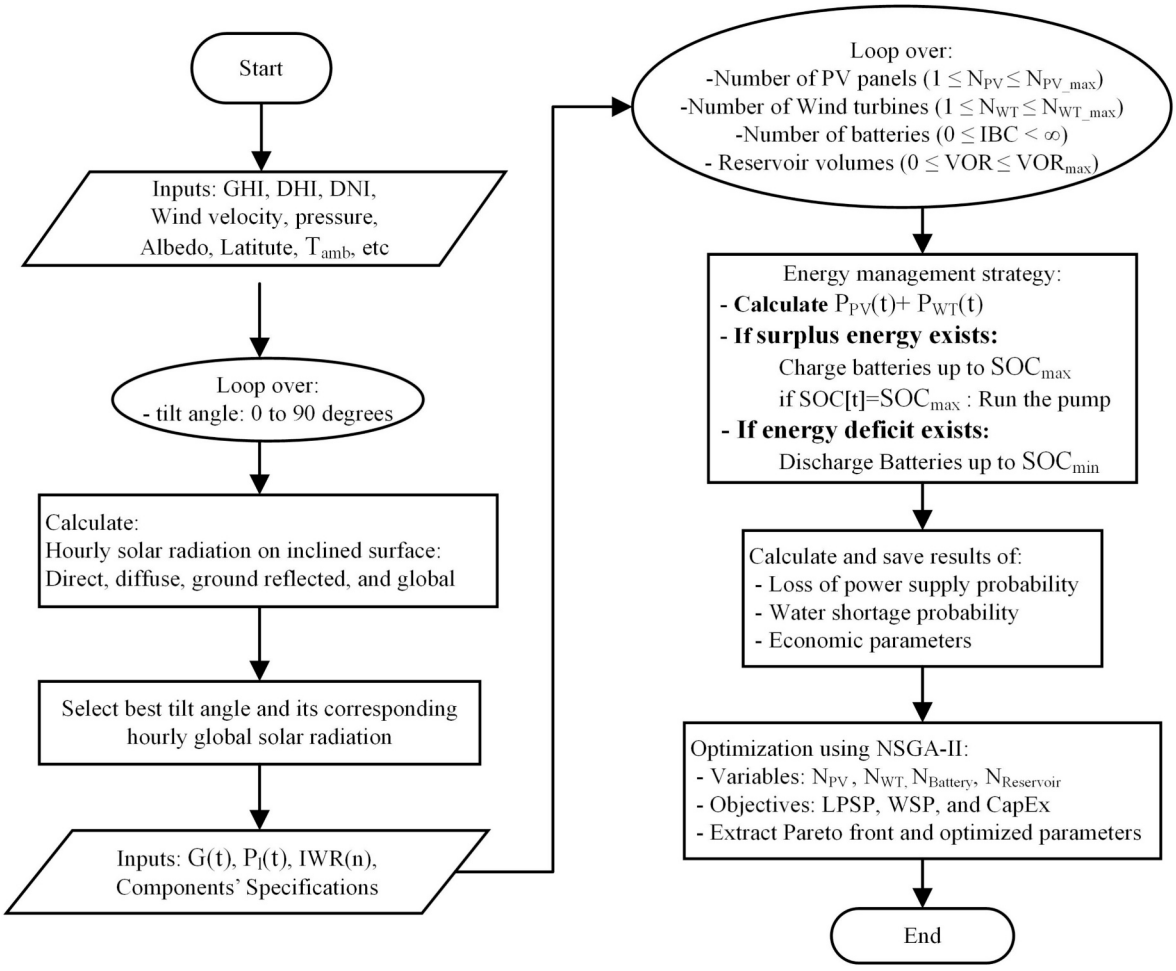

Fig. 2. Algorithm used in the study.

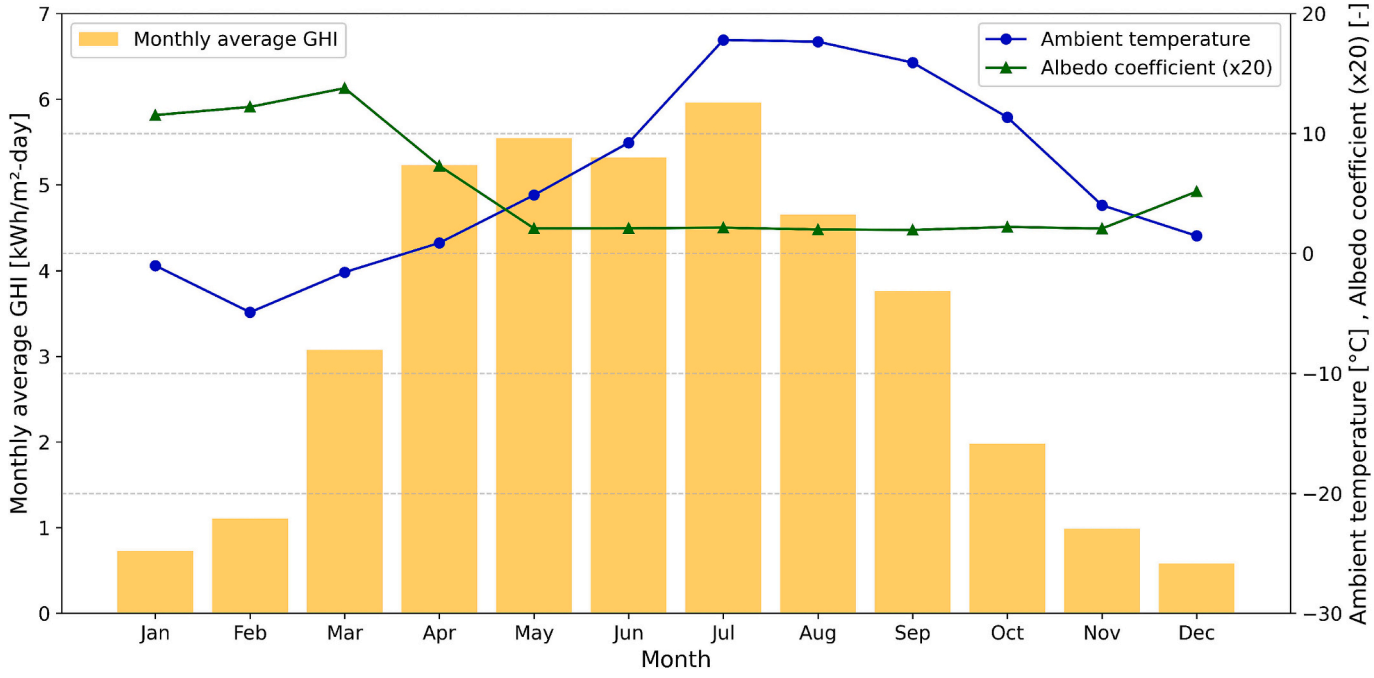

Fig. 3. Monthly averages of GHI, ambient temperature, and albedo coefficient for Îles-de-la-Madeleine, QC. Data from the NSRDB [14].

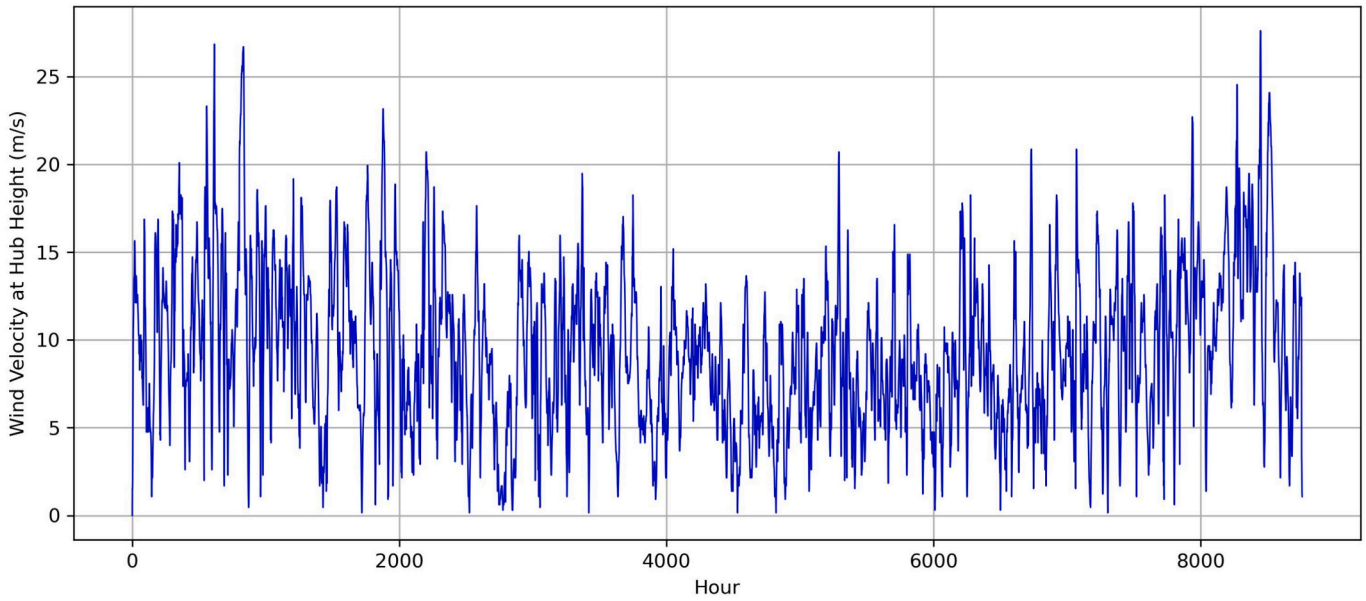

Fig. 4. Typical windspeed at hub height for Îles-de-la-Madeleine, QC [14].

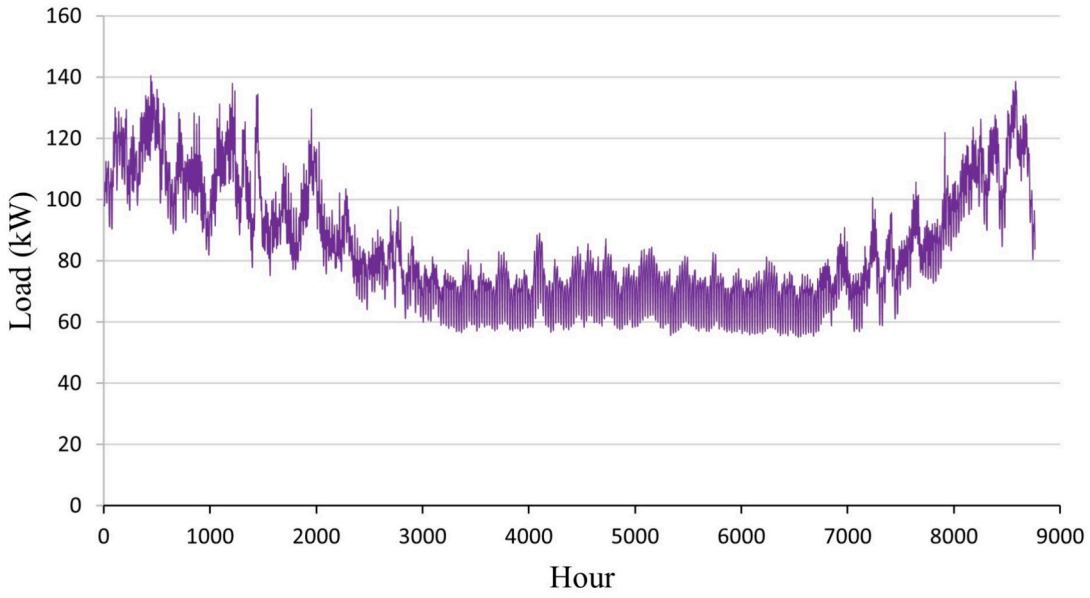

Fig. 5. Electricity load demand profile.

where the exponent (α), an empirical coefficient, is assumed to be 1/7 [24]. Finally, the actual output power of a WT is calculated using the following equation:

$$P_{WT} = \left(\frac{\rho}{\rho_0}\right) \times P_{WT,STP} \tag{6}$$

where ρ_0 is the air density at STP conditions, which equals 1.225 kg/m^3. The actual density of air is derived from the ideal gas law. It is also assumed that the maximum number of wind turbines ($N_{WT,max}$) could be 26, i.e.:

$$0 \leq N_{WT} \leq N_{WT,max} \tag{7}$$

4.3. Battery storage system

The following equations define the dispatch strategy for PV, WT, and batteries:

$$P_b(t) = P_{PV}(t) + P_{WT}(t) - P_{l,real} \tag{8}$$

$$P_{l,real} = \frac{P_l(t)}{\eta_{inv}} \tag{9}$$

where $P_{l,real}$ is the power passing through the inverter [25], and $P_l(t)$ is the load demand at each hour. When $P_b(t) > 0$, surplus energy is available, and the batteries' State of Charge (SOC) is determined using the following equation [25]:

$$SOC_{Charging}(t) = SOC(t-1) \times (1-\sigma) + (P_b(t) \times \eta_{bc}) / IBC \tag{10}$$

On the other hand, when $P_b(t) < 0$, there is an energy deficit, and the State of Charge (SOC) is determined using the following equation [25]:

$$SOC_{Discharging}(t) = SOC(t-1) \times (1-\sigma) + (P_b(t) \times \eta_{bd}) / IBC \tag{11}$$

where σ, η_{bc}, and η_{bd} represent the self-discharge rate and the battery efficiency under charging and discharging conditions, respectively. For simplicity, self-discharge rate is assumed to be 0 and the efficiency of 1 were considered in this study. The nominal installed battery capacity (IBC) is calculated using the following equation:

$$IBC = N_{Battery} \times C_{Battery} \quad (12)$$

where $C_{Battery}$ is the nominal capacity of each battery in Wh. Unlike the PV panels, no limitation on the number of possible batteries was considered; therefore:

$$0 \leq IBC < \infty \quad (13)$$

Therefore, a very large number of battery banks was considered as the upper bound. The batteries are also assumed to have high charging/discharging rates. In addition, the initial state of charge of the batteries was set to 50 %, which is a commonly adopted neutral starting point in hybrid renewable energy system simulations to avoid optimistic (fully charged) or pessimistic (fully depleted) bias; similar assumptions have been employed in recent studies by Wongdet et al. [26], Vega-Garita et al. [27], and Shaker et al. [28]:

$$SOC(0) = 0.5 \quad (14)$$

It should be noted that lower and upper bounds for the SOC of the batteries must be considered during system design to prevent over-charging or over-discharging, which helps extend battery lifespan. The SOC_{min} and SOC_{max} values are set at 10 % and 90 %, respectively:

$$0.1 \leq SOC(t) \leq 0.9 \quad (15)$$

4.4. Water pumping system

A centrifugal pump (Lorentz PS2–4000C-SJ17–4) with DC motor and nominal power of 4 kW is selected. Its characteristic curve was derived from the manufacturer datasheet [29]. The Curve Fitter tool in MATLAB [30] was used to derive the characteristic curve equation. The pump's flow rate (Q [m^3/h]) at different heads (H [m]) and input powers (P [W]) are calculated as follows:

$$Q = Q_{00} + Q_{10} \times H + Q_{01} \times P + Q_{20} \times H^2 + Q_{11} \times H \times P + Q_{02} \times P^2 \quad (16)$$

where $Q_{00} = 3.276$, $Q_{10} = -0.6048$, $Q_{01} = 0.01748$, $Q_{20} = -0.0007923$, $Q_{11} = 0.0001245$, and $Q_{02} = -3.137 \times 10^{-6}$. The goodness of the fitted curve was evaluated using R^2, which was equal to 0.9935. The curve and the residual values are shown in Fig. 6. Using this equation, the amount of pumped water throughout the day can be calculated. It is worth noting that, based on the datasheet, the pumping system has a minimum power requirement below which the pump cannot operate (see Table 1). Furthermore, the system limits the input power of the pumping system and this power is different for each head. In this study, a total head of 45 m was assumed for the pumping system.

4.5. Water storage system

Considering an analogy between the battery storage system and water storage tanks, the Volume Of Reservoirs for each day (VOR(n)) is calculated based on the difference between daily pumped water (V(n)) and daily Water Requirement (WR(n)):

$$VOR(n) = VOR(n-1) + \sum_{t=1}^{t=24} Q(t) - WR(n) \quad (17)$$

As mentioned in Section 3. Case study, a constant daily water requirement of 26 m^3 was considered for the community. Each water storage tank occupies a certain area and this necessitates putting a limit

Table 1
Minimum and maximum power ranges for the Lorentz PS2–4000C-SJ17–4 pump at different heads [29].

Head [m]	10	15	20	25	30	35	40	45
Minimum input power [kW]	0.15	0.32	0.50	0.70	0.90	1.07	1.21	1.41
Maximum input power [kW]	3.50	3.50	3.50	3.50	3.40	3.35	3.35	3.30

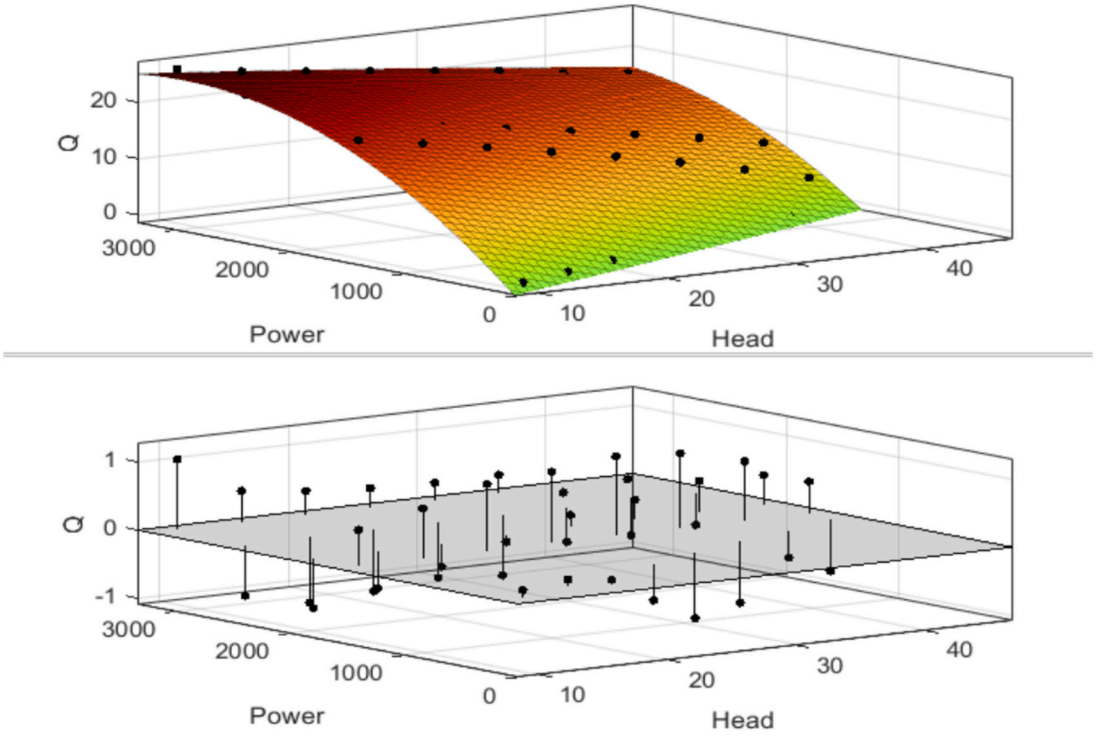

Fig. 6. The fitted pump characteristic curve (top) and its residual values (bottom).

on the maximum number of water storage tanks. Based on the type of water storage selected and area limitations, a maximum reservoir volume (VOR_{max}) of 87 m^3 was considered:

$$0 \leq VOR < VOR_{max} \tag{18}$$

It is worth mentioning that the surplus pumped water is curtailed.

4.6. Reliability models

LPSP is used as a criterion for assessing the reliability of electricity supply for the community. The LPSP is defined as follows [25]:

$$LPSP = \frac{\sum_{t=1}^{t=8760} LPS(t)}{\sum_{t=1}^{t=8760} P_l(t)} \times 100 \tag{19}$$

Based on the users' tolerance, a maximum allowable power loss will be considered:

$$LPSP < LPSP_{max} \tag{20}$$

The WSP percentage which is a measure of water access reliability [7] is defined as:

$$WSP\ (\%) = \frac{\sum_{d=1}^{d=365} WS(d)}{\sum_{d=1}^{d=365} WR(d)} \times 100 \tag{21}$$

Similarly, a maximum value for the maximum WSP will be considered:

$$WSP < WSP_{max} \tag{22}$$

4.7. Economic model

The life cycle cost of the project was analyzed in this study. It is defined as follows:

$$\text{Life Cycle Cost} = CapEx + OpEx_t \tag{23}$$

where CapEx and $OpEx_t$ are the capital expenditure and total annual operational expenditures, respectively, and are defined as follows [5]:

$$\begin{aligned} CapEx = {} & CapEx_{PV} + CapEx_{WT} + CapEx_{Battery} + CapEx_{Pumping} \\ & + CapEx_{Inverter} + CapEx_{MPPT} + CapEx_{Reservoir} \end{aligned} \tag{24}$$

Similar to WSP_{max} and $LPSP_{max}$, a maximum value is considered for CapEx:

$$CapEx < CapEx_{max} \tag{25}$$

The total annual operational expenditures are defined as follows [5]:

$$OpEx_t = M_t + R_t + O_t + F_t \tag{26}$$

The operational cost (O_t) and fuel cost (F_t) are assumed to be zero. Furthermore, the maintenance cost (M_t) is considered to be 2 % of the initial costs of the pumping system and PV panels each year throughout the project's lifetime [5,31] and a constant value of 600 $ is considered for WT maintenance. The components' salvage values are disregarded, assuming they will be utilized throughout their entire lifespan [32–34]. Furthermore, the lifetime of the project was assumed to be 30 years. The replacement cost is determined based on the components' lifespan as follows:

$$\begin{aligned} R_t = {} & \left(CapEx_{Battery} + CapEx_{Inverter} + CapEx_{MPPT} + CapEx_{Pump}\right) \\ & \times \left(\frac{1}{(1+r)^{10}} + \frac{1}{(1+r)^{20}}\right) + \left(CapEx_{WT} \times \frac{1}{(1+r)^{15}}\right) \end{aligned} \tag{27}$$

The discount rate (r) is assumed to be 4 % based on the reports of Bank of Canada [35]. Furthermore, payback period is also considered to assess the feasibility of the project [23,36]:

$$\text{Payback period} = \frac{CapEx}{\text{Return} - \text{Annualized } OpEx_t} \tag{28}$$

Return represents the cost savings from avoiding diesel generator fuel and its corresponding costs and is calculated as:

$$\begin{aligned} \text{Return} = {} & [\text{Annual Energy Consumed} \times \text{Fuel price} \times \text{DG Efficiency}] \\ & + DG_{OM} + DG_{Price} \end{aligned} \tag{29}$$

where Annual Energy Consumed is the total residential load and power required for pumping water. Diesel fuel price is considered to be equal to 1.78C$/L [37] and a mean value of 0.71 L/kWh is considered for the diesel generator efficiency assuming a 50 % capacity utilization for the DG [38]. Furthermore, its O&M costs estimated from available DGs on the market is assumed to be C$200 per year.

The optimization problem in the study is of a multi-objective type. As shown in the algorithm chart, there are four design variables (N_{PV}, N_{WT}, $N_{Battery}$, VOR_{max}) and three objectives (LPSP, WSP, and CapEx). The goal is to minimize these objectives, that results in higher reliability in load and water demand, as well as lower costs. A multi-objective framework is used to minimize the objectives. The optimization is based on real data and configurations, therefore, a large dataset of different possible combinations of design is used. In this approach, only combinations meeting the defined constraints are considered in the optimization:

$$LPSP < LPSP_{max} \tag{30}$$

$$WSP < WSP_{max} \tag{31}$$

$$CapEx < CapEx_{max} \tag{32}$$

The NSGA-II method [39] is used to solve this multi-objective problem by using DEAP algorithm [40] of python's NumPy package [41]. To ensure reproducibility, the multi-objective optimization was performed using NSGA-II with a population size of 1000 over 1000 generations. A uniform crossover operator was applied with a probability of 0.7 (gene-level probability 0.5), and mutation was performed with a probability of 0.2. These values were selected based on recommended ranges in the literature to balance exploration and exploitation while maintaining computational efficiency. Selection followed the standard NSGA-II procedure with non-dominated sorting and crowding distance to preserve solution diversity. A fixed random seed (100) was used to guarantee consistent results across runs. Each candidate solution was evaluated against the three objective functions(i.e. minimizing LPSP, WSP, and CAPEX) while respecting key system constraints such as battery state-of-charge limits, reservoir capacity, and maximum allowable PV/WT numbers. The final output of the algorithm is a Pareto front of optimal solutions, offering a set of trade-offs rather than a single solution. It is important to note that the NSGA-II multi-objective optimization does not yield a single “best” solution; rather, it generates a Pareto front of non-dominated solutions. This allows the decision-makers to choose the most appropriate configuration based on the desired trade-off between cost, reliability, and water availability.

5. Specifications of the components

In this section, the specifications of the main components (i.e., PV panels, wind turbines, batteries, inverter, pumping system, water storage system, and solar charge controller) are summarized in Table 2. The project duration is set at 30 years, and the lifespans of the batteries, inverter, and charge controller are assumed to be 10 years. The PV panels, and water storage system are assumed to operate for the life time of the project. The price of each component listed in the table is presented in Canadian dollars and estimated from the market.

Table 2
Specifications of the components.

PV model	RESTAR RTM-100 M [42]
Type	Mono-crystalline
Power at STC, P_{mp}	100 W
Voltage at P_{mp}	17.90 V
Current at P_{mp}	5.59 A
Module Efficiency	15.44 %
Temperature Coefficient of P_{mp}	−0.39 %/°C
NOCT	45 °C
Lifespan	30 years
Dimensions	1200 × 540 × 35 mm
Price	C$150

Wind turbine	Bergey windpower Excel 10 [43]
Type	Horizontal axis with 3 blades
Rated Power	8.9 kW
Rated Windspeed	11 m/s
Cut-in Windspeed	2.5 m/s
Cut-out Windspeed	N.A. (assumed to be 20)
Lifespan	15 years
Price	C$40000

Battery model	DC HOUSE [44]
Type	Deep cycle lithium
Battery Capacity	2.56 kWh
Lifespan	10 years
Price	C$550

Inverter	Generic model
Type	Pure sine wave
Maximum Efficiency	92 %
Lifespan	10 years
Price	20 % of PV + WT system

Charge controller	Generic model
Type	MPPT
Lifespan	10 years
Price	20 % of PV system

Pumping system	Lorentz PS2-4000 C-SJ17-4 [29]
Type	Submersible
Maximum Power	4 kW
Maximum Flow Rate	26 m^3/h
Maximum Head	45 m
Lifespan	10 years
Price	C$10000

Water storage	VT1650-86 [45]
Type	Vertical liquid storage tank
Volume	6246 Liters
Dimensions	86″ Diameter x 74″ Height
Lifespan	30 years
Price	C$2500

6. Results and discussions

The study by Bhayo et al. [5] was used for validation purposes, and the details of the validation process were provided in the study of Irandoostshahrestani and Rousse [7], ensuring the validity of the results for basic solar geometric equations, PV/battery calculations, and the developed economic model. Initially, it is important to find the most appropriate tilt angle for the PV array. Although there are general guidelines for finding the best tilt angle, various factors like the location's latitude, surface azimuth angle, clearness index, etc. affect the optimal slope [46]. Three different modes were considered to determine the best angle: (1) a fixed tilt angle throughout the year, (2) a seasonal adjustment of the tilt angle to its optimal value, and (3) a monthly adjustment of the tilt angle to its best value for each month. In all different modes, various tilt angles from 0° to 90° were evaluated to obtain the optimum angle in terms of the average global solar radiation

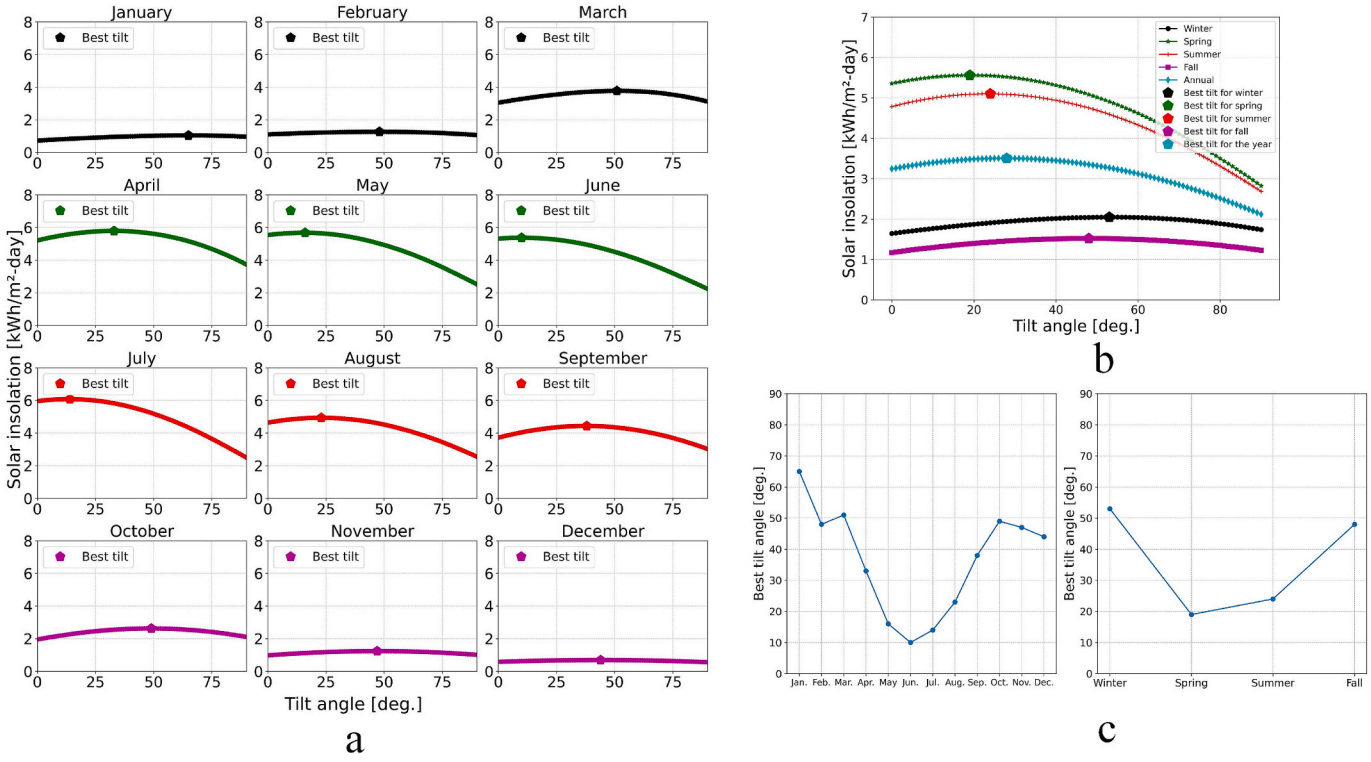

Fig. 7. Monthly solar insolation and optimal tilt angles. (b) Seasonal and annual tilt optimization. (c) Optimized monthly and seasonal tilt angles.

on the inclined surface. Fig. 7 shows the result of solar insolation and the optimized tilt angle for the mentioned modes. Fig. 7(a) shows that the optimal tilt angles vary considerably during the year, and they range from 10° in June to 65° in January. As shown in Fig. 3, July has the highest GHI values, making it the month with the greatest solar insolation among other months in Fig. 7(a). Similarly, solar insolation is generally higher in spring and summer but significantly weaker in fall and winter due to lower GHI values, as shown in Fig. 7(b). This figure shows that a fixed tilt angle of 28° results in a maximum annual insolation of 3.50 kWh/m^2-day. For monthly and seasonally changing tilt angle modes, the best tilt angles are shown in Fig. 7(c). Fig. 8 depicts the daily average of solar insolation for the three modes, showing that the annual average of daily solar insolation for a fixed 28° tilt angle (3.50 kWh/m^2-day) is only slightly lower than that of the seasonal (3.56 kWh/m^2-day) and monthly (3.59 kWh/m^2-day) adjustment modes. This corresponds to a maximum reduction of 2.6 % in annual insolation for the

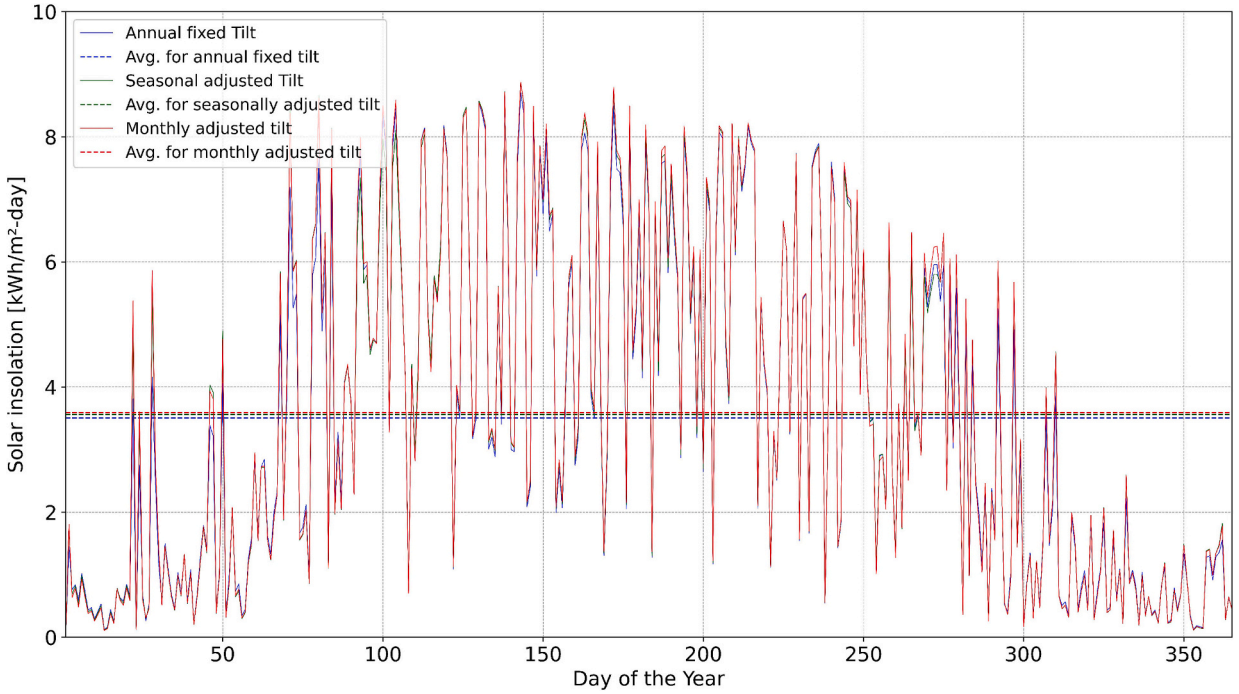

Fig. 8. Comparison of solar insolation for fixed, seasonal, and monthly tilt adjustment strategies throughout the year.

fixed tilt angle strategy. Although monthly tilt adjustment yields slightly higher energy capture, the additional labor and operational complexity may outweigh the benefits. Therefore, for this study, a fixed tilt strategy was adopted to simplify system operation and ensure practicality for remote communities. Fig. 8 shows that solar insolation is considerably lower in fall and winter, and it emphasizes the importance of wind turbine contributions during low-irradiation months.

The results of the optimization, with constraints of $LPSP_{max}$ and WSP_{max} set at 15 % and $CapEx_{max}$ set at 3,000,000C$, are shown in Fig. 9. Each point in the top plot represents a Pareto-optimal solution, where LPSP is shown on the x-axis, CapEx on the y-axis, and WSP is indicated by the color scale. The bottom 3-D plot shows the corresponding system configurations (number of PV modules, wind turbines, and batteries) for these solutions, allowing readers to visualize how different component combinations achieve the trade-off between cost, reliability, and water availability. All the solutions correspond to systems with 180 to 230 kW of wind turbine rated power, 30 to 60 kW capacity of PV panels, and 1 to 3.6 MWh battery storage and 68–87 m^3 of water storage system (not shown in the figures), approximately. Furthermore, most of the optimized systems feature the maximum possible number of PV panels and battery capacities up to 3.6 MWh although there were no constraint for battery capacity. This is because batteries impact the system's CapEx more than other components due to their higher prices; therefore, the optimized systems tend to include a limited capacities for battery banks. These results highlight that even modest increases in system investment can yield disproportionately large improvements in reliability, a critical consideration for remote communities where power and water shortages have direct social and economic impacts. For instance, increasing the total investment from 1.8 M CAD to 2.2 M CAD (approximately a 33 % increase) reduces the loss of power supply probability from 14 % to 6 %, representing a considerable improvement in system reliability.

To demonstrate the performance of the designed system, a system configuration of interest with 60 kW PV panel capacity, 231.4 kW nominal power of WT, 1.54 MWh battery storage capacity, and a water storage volume of 87 cubic meters, resulting in an LPSP of 9.9 %, WSP of 5.4 %, and a CapEx of M$ 2.2 is selected. The system performance is shown in Fig. 10. Despite low solar insolation in cold seasons and low WT power generations in some days, the system remains reliable by means of the battery storage systems that leads to minimum SOCs for the batteries at many hours of the year. Furthermore, the daily water requirement, pumped water, reserved water, and water deficit throughout the year are shown in Fig. 11. It is evident that there is abundant excess power in most of the year with a maximum potential pumped water of 384 m^3 as the pumping system has maximum water pumping rate of 16 m^3 per hour at full load. Here, the WSP is mainly limited by the maximum water storage capacity, as there is considerable excess power, and increasing storage capacity can help mitigate water shortages.

To better understand the contribution of each energy production

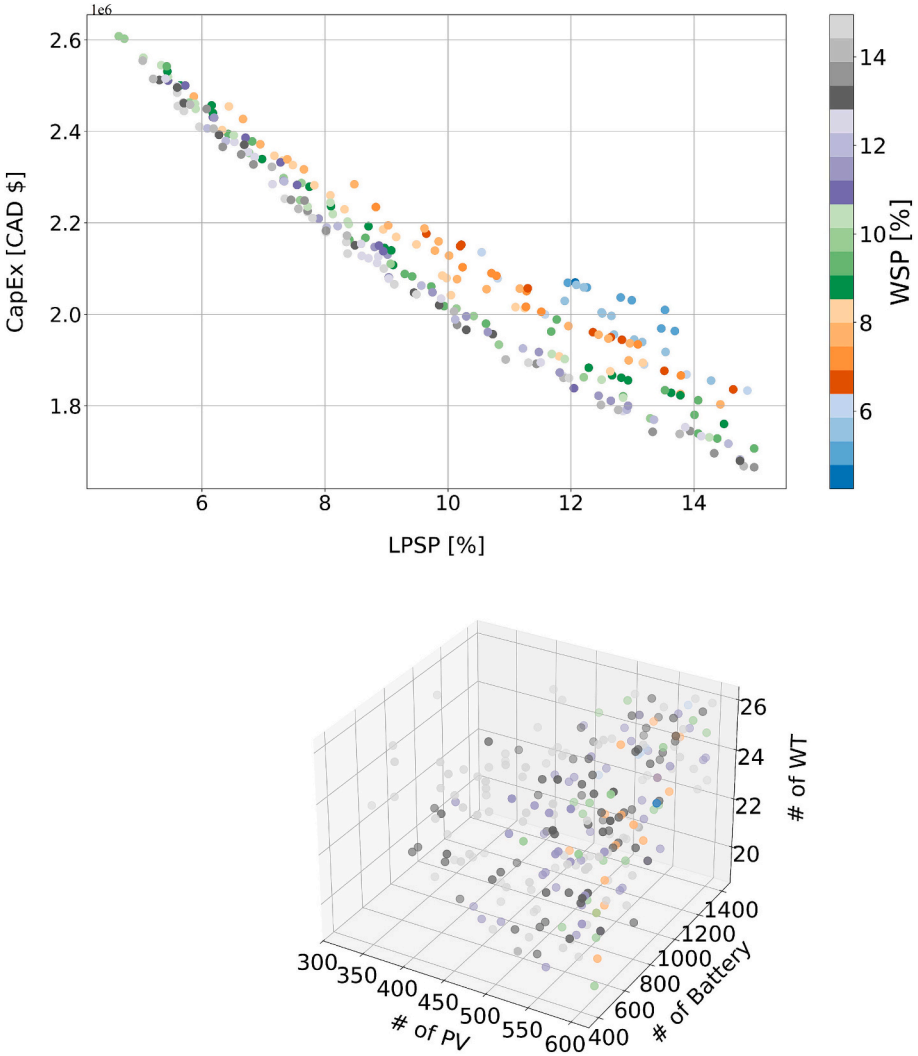

Fig. 9. Optimized objectives (top) and the corresponding system configuration (bottom) for $LPSP_{max}$ and WSP_{max} of 15 % and $CapEx_{max}$ of 3 M$.

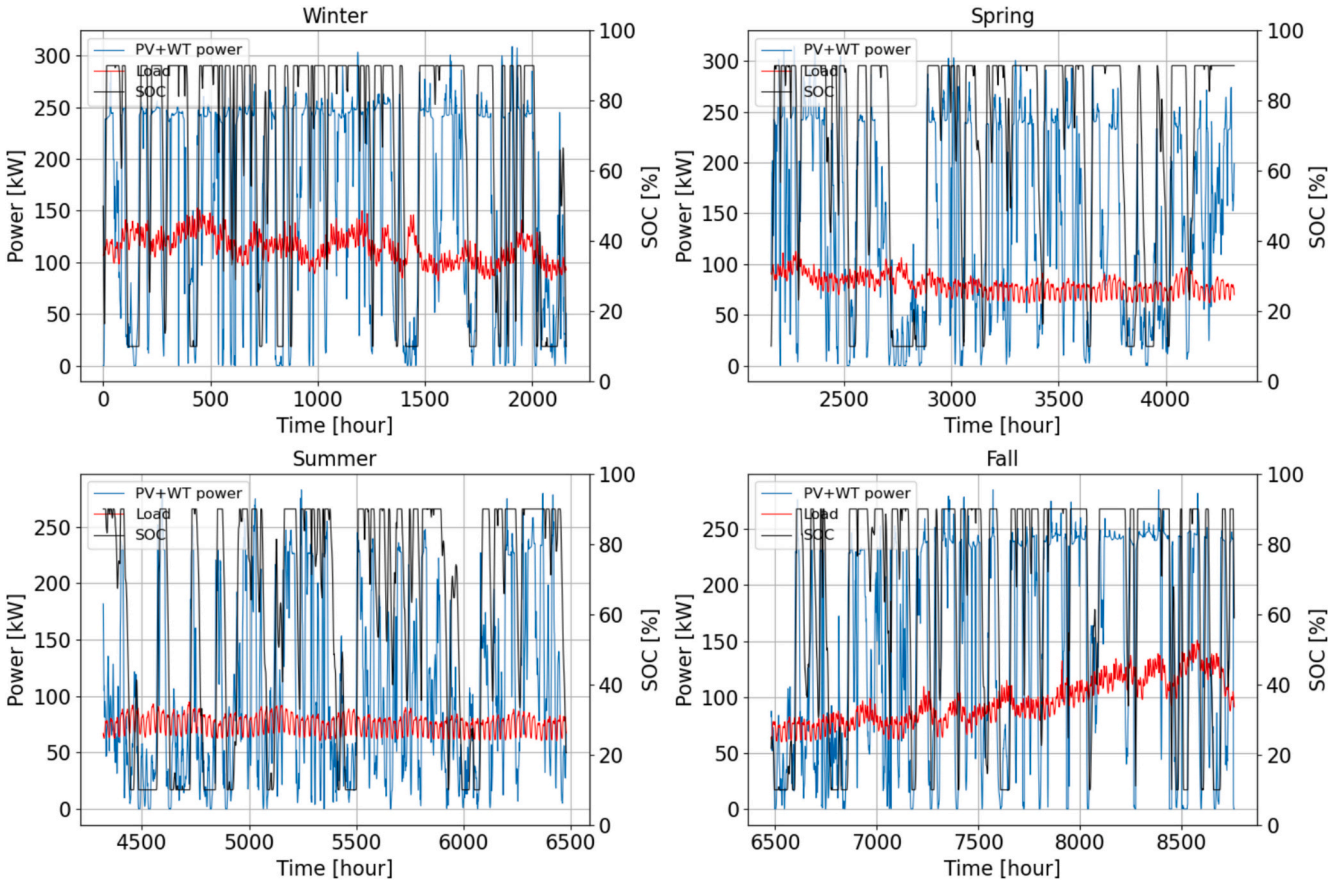

Fig. 10. SOC, PV and WT generated power, and load demand over the course of a year for a specific system.

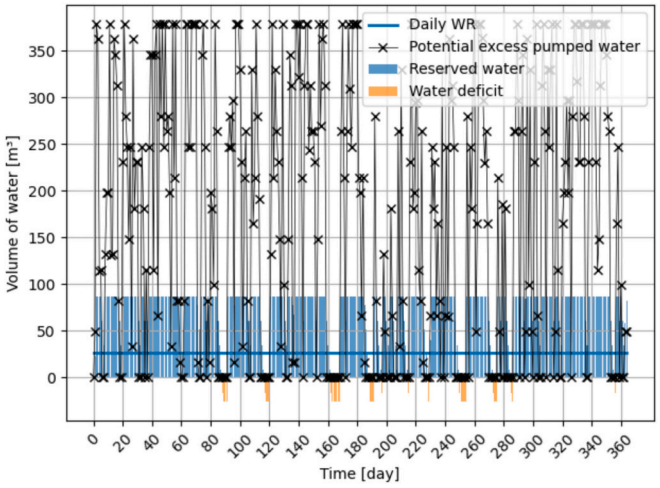

Fig. 11. Water volume dynamics during the year for a specific system.

source, Fig. 12 depicts the daily average energy production for the mentioned system (i.e., a system with a 231.4 kW wind turbine and 60 kW PV capacity with 1.54 MWh battery storage and a 87 m^3 water tanker). The blue bars represent wind turbine production, while the yellow sections indicate solar PV generation. It is evident that the wind contribution is considerably higher than solar since the installed capacity of the wind turbine system is significantly higher. The red dashed line is the average daily energy consumption. There are times when total renewable generation is more than consumption, and also other times when production is low, that shows the variability of these energy sources. In summer, when wind speeds are low (see Fig. 4), solar PV production compensates the low wind energy productions. On the other hand, in seasons with less sunlight, wind production is higher and it makes up the low solar energy generations. It demonstrates how wind and solar energy complement each other throughout the year, and they create a more balanced and reliable system compared to systems relying only on PV or WT generation. It is worth mentioning that the nominal power of PV system is lower than WT installations as they occupy more area. Systems with a single electricity source can only operate effectively when the source is stable and the demand is lower than the generation capacity. This is evident in the study by Bhayo et al. [5], where the maximum hourly load was <300 W, and there were no consecutive days of very low irradiation in the case study of Malaysia. It is worth noting that the system corresponding to Fig. 12 has an LPSP of 9.9 % and a WSP of 5.4 %, with a CapEx of M$2.2. The mentioned complementary behavior of PV and WT relatively minimizes the need to oversize the system with excessively large PV panels, wind turbines or storage. It is obvious that it is possible to design a system with LPSP of zero but it requires a larger system size. However, the goal of this study is to show the feasibility of increasing renewable energy penetration while keeping in mind that an auxiliary power generation system should be considered to enhance system reliability.

In order to evaluate the economic feasibility of the project, the payback period is plotted for the optimized solutions, Fig. 13. It can be seen that the system with the lowest LPSP has a payback period of 12.0 years, while systems with an LPSP of 15 % have payback periods of about 8.0 years. It should be mentioned that these payback period values are obtained based on scenarios where a diesel generator is used as an alternative to the renewable PV/WT system and the land price is not included in the calculations. However, when access to the grid is available, the payback period for renewable systems increases, making

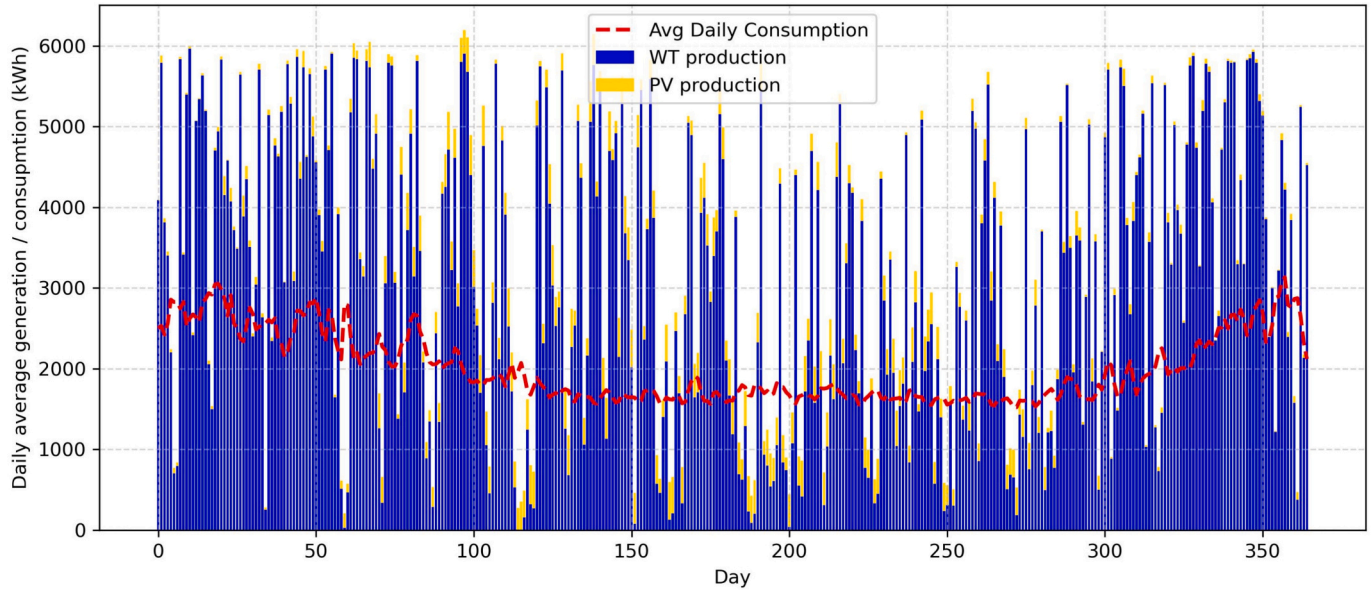

Fig. 12. Daily total energy production from PV and WT over a year for a specified configuration.

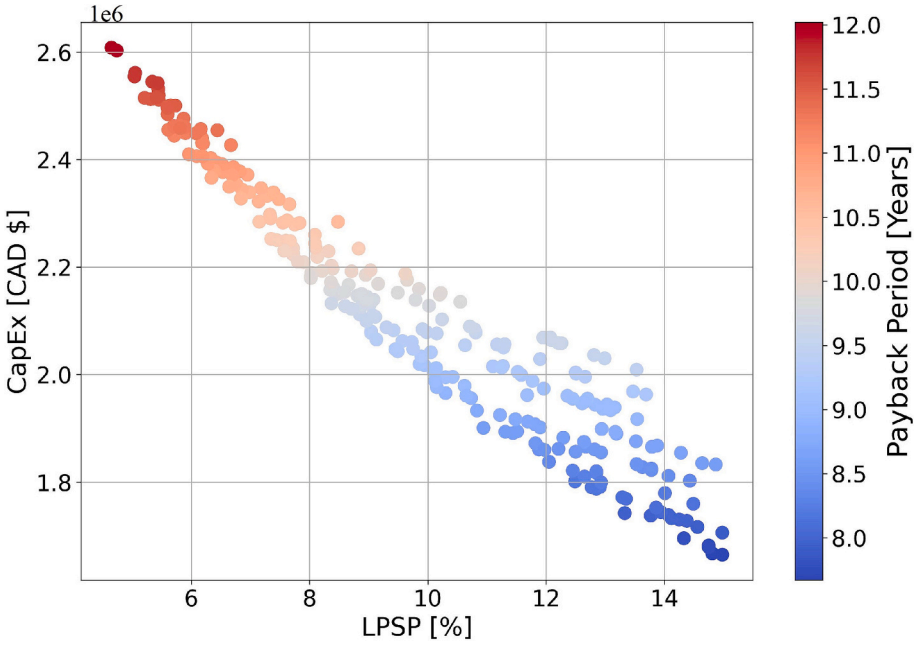

Fig. 13. Payback period for proposed systems.

them unfeasible due to the considerably low electricity price in Quebec [47], which is around 6.7 cents per kWh. The proposed systems of the study have LCOE in the range of 16.3 ¢/kWh to 23.4 ¢/kWh that are not competitive with grid power in Quebec. However, Îles-de-la-Madeleine has no grid access as it is located >100 km away from the coast of Quebec and the calculation of the payback is not based on grid electricity.

7. Conclusions

In this study, an off-grid PV-WT-battery and water storage system is designed to meet the residential load demand and provide water for a community in Îsles de la Madeleine, Quebec, Canada. The EMS used in the study prioritizes residential load demand over water pumping. The EMS mandates that the system charge the batteries when excess power is available after meeting the residential load. Furthermore, if surplus energy still remains, the pumping system is activated to store water in reservoirs. The concepts of LPSP and WSP are employed to evaluate system reliability, and the system is optimized using the GA with these reliability objectives, as well as CapEx. Due to land area limitations, the system design imposes a maximum allowable number of PV panels and wind turbines. It was shown that the electricity production of PV and WT exhibits complementary behavior across different seasons, enhancing system reliability. It was demonstrated that LPSP and WSP significantly influence system size and, consequently, its CapEx. Furthermore, the system has considerable excess power during the year which can be used for water pumping system for the community. The goal of this study was to show the feasibility of increasing renewable energy systems in remote areas with no grid access in order to lower dependancy to conventional diesel generator power generation. The proposed optimized systems had

a payback period in the range of 8.0 to 12.0 years with LCOE in the range of 16.3 ¢/kWh to 23.4 ¢/kWh. This work provides a practical decision-support framework that enables planners and community stakeholders to select the most appropriate configuration based on desired trade-offs between cost, electricity reliability, and water security.

CRediT authorship contribution statement

Misagh Irandoostshahrestani: Writing – review & editing, Writing – original draft, Visualization, Validation, Software, Methodology, Investigation, Formal analysis, Data curation, Conceptualization. **Daniel R. Rousse:** Writing – review & editing, Validation, Supervision, Resources, Project administration, Methodology, Investigation, Funding acquisition, Formal analysis, Conceptualization.

Declaration of Generative AI and AI-assisted technologies in the writing process

During the preparation of this work the authors used ChatGPT in order to improve the readability and language of the manuscript. After using this tool, the authors reviewed and edited the content as needed and take full responsibility for the content of the published article.

Funding sources

The authors would like to acknowledge the support provided for this research by the Fonds de recherche du Québec – Nature et technologies (FRQ-NT) through the Programme de bourses d'excellence pour étudiants étrangers (PBEEE).

Declaration of competing interest

The authors declare the following financial interests/personal relationships which may be considered as potential competing interests: Misagh Irandoostshahrestani reports financial support was provided by Quebec Research Fund Nature and Technology. Daniel R. Rousse reports financial support was provided by Quebec Research Fund Nature and Technology. If there are other authors, they declare that they have no known competing financial interests or personal relationships that could have appeared to influence the work reported in this paper.

Appendix A

In this section, basic solar geometric equations are presented, as derived from the reference book by Duffie and Beckman [48]. The declination angle, in degrees, is calculated using the approximate equation by Cooper [49]:

$$\delta = 23.45 \times \sin\left(360 \times \frac{284 + n}{365}\right) \tag{A-1}$$

where n is the day number (e.g., $n = 1$ for January 1st). The hour angle, in degrees, is defined as:

$\omega = 15 \times$ (12-ST) (A-2).

where ST is the solar time, calculated using the following equation:

$$ST = LT + \frac{(EOT + 4 \times (LL - LSTM))}{60} \tag{A-3}$$

where LT is the local time, LL is the longitude, LSTM is the local standard time meridian, and equation of time (EOT) is determined by:

$$EOT = 229.2 \times (0.000075 + 0.001868 \times \cos(B) - 0.032077 \times \sin(B) - 0.014615 \times \cos(2B) - 0.04089 \times \sin(2B)) \tag{A-4}$$

and Γ is given by:

$$\Gamma = 360 \times \frac{(n - 81)}{365} \tag{A-5}$$

The zenith angle and the angle of incidence are defined, respectively, as:

$$\theta_z = \arccos(\sin(\delta) \times \sin(\varphi) + \cos(\delta) \times \cos(\varphi) \times \cos(\omega)) \tag{A-6}$$

$$\theta = \arccos(\theta_1 + \theta_2 + \theta_3) \tag{A-7}$$

and θ_1, θ_2, and θ_3 are given by:

$$\theta_1 = (\sin(\varphi) \times \cos(\beta) - \cos(\varphi) \times \sin(\beta) \times \cos(\gamma)) \times \sin(\delta) \tag{A-8}$$

$$\theta_2 = (\cos(\varphi) \times \cos(\beta) + \sin(\varphi) \times \sin(\beta) \times \cos(\gamma)) \times \cos(\delta) \times \cos(\omega) \tag{A-9}$$

$$\theta_3 = \cos(\delta) \times \sin(\beta) \times \sin(\gamma) \times \sin(\omega) \tag{A-10}$$

where φ, β and γ represent the latitude, tilt angle, and azimuth angle, respectively. The hourly global solar radiation (G) in W/m^2 on an inclined surface is calculated using the isotropic diffuse model by Liu and Jordan [50]:

$$G_\beta = DNI \times \cos\theta + DHI \times \left(\frac{1 + \cos(\beta)}{2}\right) + GHI \times \mu \times \left(\frac{1 - \cos(\beta)}{2}\right) \tag{A-11}$$

where μ is the albedo coefficient and the Global Horizontal Irradiance (GHI) is calculated using the Direct Normal Irradiance (DNI), and Diffuse Horizontal Irradiance (DHI) as follows:

$$GHI = DNI \times \cos(\theta_z) + DHI \tag{A-12}$$

Data availability

Data will be made available on request.

References

[1] L. Cozzi, D. Wetzel, G. Tonolo, N. Diarra, A. Roge, Access to electricity improves slightly in 2023, but still far from the pace needed to meet SDG7, IEA (2023). Accessed: Jan. 14, 2025. [Online]. Available: https://www.iea.org/commentaries/access-to-electricity-improves-slightly-in-2023-but-still-far-from-the-pace-needed-to-meet-sdg7.

[2] IRENA, IRENA, *Renewable Power Generation Costs in 2020, International Renewable Energy Agency*. Abu Dhabi, 2021, Accessed: Jan. 14, 2025. [Online]. Available: https://www.irena.org/-/media/Files/IRENA/Agency/Publication/2021/Jun/IRENA_Power_Generation_Costs_2020.pdf, *2021*.

[3] S. Meunier, et al., A validated model of a photovoltaic water pumping system for off-grid rural communities, Appl. Energy 241 (2019) 580–591, https://doi.org/10.1016/j.apenergy.2019.03.035.

[4] Y. Bakelli, A. Hadj Arab, B. Azoui, Optimal sizing of photovoltaic pumping system with water tank storage using LPSP concept, Sol. Energy 85 (2) (2011) 288–294, https://doi.org/10.1016/j.solener.2010.11.023.

[5] B.A. Bhayo, H.H. Al-Kayiem, S.I. Gilani, Assessment of standalone solar PV-Battery system for electricity generation and utilization of excess power for water pumping, Sol. Energy 194 (2019) 766–776, https://doi.org/10.1016/j.solener.2019.11.026.

[6] D.H. Muhsen, A.B. Ghazali, T. Khatib, Multiobjective differential evolution algorithm-based sizing of a standalone photovoltaic water pumping system, Energ. Convers. Manag. 118 (2016) 32–43, https://doi.org/10.1016/j.enconman.2016.03.074.

[7] M. Irandoostshahrestani, D.R. Rousse, Photovoltaic electrification and water pumping using the concepts of water shortage probability and loss of power supply probability: a case study, Energies (Basel) 16 (1) (2023), https://doi.org/10.3390/en16010001.

[8] A. El-Maaroufi, M. Daoudi, R. Ahl Laamara, Optimal design and techno-economic analysis of a solar-wind hybrid power system for laayoune city electrification with hydrogen and batteries as a storage device, Phys. Chem. Earth 136 (2024), https://doi.org/10.1016/j.pce.2024.103719.

[9] Z. Al-Omari, N. Khlaifat, M. Haddad, A feasibility study of combining solar/wind energy to power a water pumping system in Jordan's Desert/Al-Mudawwara village, Environ. Sustain. Indic. (2024), https://doi.org/10.1016/j.indic.2024.100555.

[10] M. Irandoostshahrestani, D.R. Rousse, Status of photovoltaic water pumping systems in Iran: a comprehensive review, Water Sci. Technol. 89 (12) (2024) 3270–3308, https://doi.org/10.2166/wst.2024.149.

[11] A.A. Shaier, M.M. Elymany, M.A. Enany, N.A. Elsonbaty, Multi-objective optimization and algorithmic evaluation for EMS in a HRES integrating PV, wind, and backup storage, Sci. Rep. 15 (1) (2025), https://doi.org/10.1038/s41598-024-84227-0.

[12] H. Wang, Y. Li, F. Wu, S. He, R. Ding, Capacity optimization of pumped–hydro–wind–photovoltaic hybrid system based on normal boundary intersection method, Sustainability (Switzerland) 16 (17) (2024), https://doi.org/10.3390/su16177244.

[13] Y. Li, O. Li, F. Wu, S. Ma, L. Shi, F. Hong, Multi-objective capacity optimization of grid-connected wind–pumped hydro storage hybrid systems considering variable-speed operation, Energies (Basel) 16 (24) (2023), https://doi.org/10.3390/en16248113.

[14] NREL, NSRDB: The National Solar Radiation Database, Accessed: Jul. 31, 2021. [Online]. Available: https://maps.nrel.gov/nsrdb-viewer/.

[15] Gouvernement du Québec, Faits saillants sur la consommation d'eau potable, Accessed: Mar. 10, 2025. [Online]. Available: https://www.quebec.ca/agriculture-environnement-et-ressources-naturelles/eau-potable/economiser/faits-saillants.

[16] Energy Information Canada, 'High-Frequency Electricity Data: Visualization Tool (Beta)', Canadian Centre for Energy Information. Accessed: Mar. 10, 2025. [Online]. Available: https://energy-information.canada.ca/en/resources/high-frequency-electricity-data.

[17] Hydro Quebec, 'Consumption Based on the Home's Specific Features', Hydro Quebec. Accessed: Mar. 10, 2025. [Online]. Available: https://www.hydroquebec.com/residential/customer-space/electricity-use/tools/electricity-use.html.

[18] A.L. Bukar, C.W. Tan, K.Y. Lau, Optimal sizing of an autonomous photovoltaic/wind/battery/diesel generator microgrid using grasshopper optimization algorithm, Sol. Energy 188 (2019) 685–696, https://doi.org/10.1016/j.solener.2019.06.050.

[19] I.A. Ibrahim, T. Khatib, A. Mohamed, Optimal sizing of a standalone photovoltaic system for remote housing electrification using numerical algorithm and improved system models, Energy 126 (2017) 392–403, https://doi.org/10.1016/j.energy.2017.03.053.

[20] R.O. Fagbenle, J. Katende, O.O. Ajayi, J.O. Okeniyi, Assessment of wind energy potential of two sites in North-East, Nigeria, Renew. Energy 36 (4) (2011) 1277–1283, https://doi.org/10.1016/j.renene.2010.10.003.

[21] B.K. Das, M.A. Alotaibi, P. Das, M.S. Islam, S.K. Das, M.A. Hossain, Feasibility and techno-economic analysis of stand-alone and grid-connected PV/Wind/Diesel/Batt hybrid energy system: a case study, Energ. Strat. Rev. 37 (2021), https://doi.org/10.1016/j.esr.2021.100673.

[22] A. Shah Irshad, et al., Techno-economic evaluation and comparison of the optimal PV/Wind and grid hybrid system with horizontal and vertical axis wind turbines, Energy Convers. Manag. X 23 (2024), https://doi.org/10.1016/j.ecmx.2024.100638.

[23] B.K. Das, N. Hoque, S. Mandal, T.K. Pal, M.A. Raihan, A techno-economic feasibility of a stand-alone hybrid power generation for remote area application in Bangladesh, Energy 134 (2017) 775–788, https://doi.org/10.1016/j.energy.2017.06.024.

[24] M.R. Islam, R. Saidur, N.A. Rahim, Assessment of wind energy potentiality at Kudat and Labuan, Malaysia using Weibull distribution function, Energy 36 (2) (2011) 985–992, https://doi.org/10.1016/j.energy.2010.12.011.

[25] A.S. Al-Buraiki, A. Al-Sharafi, Hydrogen production via using excess electric energy of an off-grid hybrid solar/wind system based on a novel performance indicator, Energy Convers. Manag. 254 (2022), https://doi.org/10.1016/j.enconman.2022.115270.

[26] P. Wongdet, T. Boonraksa, P. Boonraksa, W. Pinthurat, B. Marungsri, B. Hredzak, Optimal capacity and cost analysis of battery energy storage system in standalone microgrid considering battery lifetime, Batteries 9 (2) (2023), https://doi.org/10.3390/batteries9020076.

[27] V. Vega-Garita, V. Alpizar-Gutierrez, F. Calderon-Obaldia, O. Núñez-Mata, A. Arguello, E. Immonen, Iterative sizing methodology for photovoltaic plants coupled with battery energy storage systems to ensure smooth power output and power availability, Energy Convers. Manag. X 24 (2024), https://doi.org/10.1016/j.ecmx.2024.100716.

[28] H.K. Shaker, H.E. Keshta, M.A. Mosa, A.A. Ali, Energy management system for multi interconnected microgrids during grid connected and autonomous operation modes considering load management, Sci. Rep. 14 (1) (2024), https://doi.org/10.1038/s41598-024-72952-5.

[29] BERNT LORENTZ GmbH & Co. KG, Solar Submersible Pump System for 6″ wells: PS2-4000 C-SJ17-4, Jan. 2022.

[30] The MathWorks Inc, MATLAB Curve Fitter Tool, R2022b, 2022. Accessed: Aug. 31, 2024. [Online]. Available: https://www.mathworks.com/.

[31] H. Li, Y. Sun, Operational performance study on a photovoltaic loop heat pipe/solar assisted heat pump water heating system, Energ. Build. 158 (2018) 861–872, https://doi.org/10.1016/j.enbuild.2017.10.075.

[32] B.P. Numbi, S.J. Malinga, Optimal energy cost and economic analysis of a residential grid-interactive solar PV system- case of eThekwini municipality in South Africa, Appl. Energy 186 (2017) 28–45, https://doi.org/10.1016/j.apenergy.2016.10.048.

[33] R. Bhandari, I. Stadler, Grid parity analysis of solar photovoltaic systems in Germany using experience curves, Sol. Energy 83 (9) (2009) 1634–1644, https://doi.org/10.1016/j.solener.2009.06.001.

[34] K. Ndwali, J.G. Njiri, E.M. Wanjiru, Multi-objective optimal sizing of grid connected photovoltaic batteryless system minimizing the total life cycle cost and the grid energy, Renew. Energy 148 (2020) 1256–1265, https://doi.org/10.1016/j.renene.2019.10.065.

[35] Bank of Canada, Bank of Canada reduces policy rate by 50 basis points to 3¼%, Accessed: Jan. 22, 2025. [Online]. Available: https://www.bankofcanada.ca/2024/12/fad-press-release-2024-12-11/, Dec. 2024.

[36] M.A. Hossain Mondal, Economic viability of solar home systems: case study of Bangladesh, Renew. Energy 35 (6) (Jun. 2010) 1125–1129, https://doi.org/10.1016/j.renene.2009.10.038.

[37] Diesel prices: global petrol prices, Accessed: Feb. 15, 2025. [Online]. Available: https://www.globalpetrolprices.com/diesel_prices/.

[38] B. Fleck, M. Huot, Comparative life-cycle assessment of a small wind turbine for residential off-grid use, Renew. Energy 34 (12) (2009) 2688–2696, https://doi.org/10.1016/j.renene.2009.06.016.

[39] K. Deb, A. Pratap, S. Agarwal, T. Meyarivan, A Fast and Elitist Multiobjective Genetic Algorithm: NSGA-II, 2002.

[40] F. Fortin, F. De Rainville, M. Gardner, M. Parizeau, C. Gagné, DEAP: evolutionary algorithms made easy, J. Open Source Softw. 2 (9) (2017).

[41] S. van der Walt, S. Colbert, G. Varoquaux, The NumPy array: a structure for efficient numerical computation, Comput. Sci. Eng. 13 (2) (2011) 22–30.

[42] https://www.restarsolar.com/mono-crystalline-panel/mono-crystalline-pan-rtm-100m.html, 'Mono crystalline pan RTM-100M', 2025.

[43] BERGEY EXCEL 10 datasheet, Accessed: Feb. 11, 2025. [Online]. Available: https://bergey.com/wp-content/uploads/excel-10-spec-sheet_2013.pdf, 2012.

[44] 12V 200Ah Deep Cycle LiFePO4 Lithium Battery, Accessed: Mar. 15, 2025. [Online]. Available: https://www.dchousepower.com/products/.

[45] ONTARIO AGRA: Vertical Liquid Storage Tanks, Accessed: Mar. 15, 2025. [Online]. Available: https://www.ontarioagra.ca/products/liquid-storage-solutions/.

[46] S. Memme, M. Fossa, Maximum energy yield of PV surfaces in France and Italy from climate based equations for optimum tilt at different azimuth angles, Renew. Energy 200 (2022) 845–866, https://doi.org/10.1016/j.renene.2022.10.019.

[47] Hydro Quebec, Electricity rates chart- 2023- Hydro Quebec, Accessed: Jan. 27, 2025. [Online]. Available: https://www.hydroquebec.com/data/documents-donnees/pdf/rates-chart-2023.pdf, 2023.

[48] J.A. Duffie, W.A. Beckman, Solar Eng. Therm. Process. 3 (3) (1982), https://doi.org/10.1016/0142-694x(82)90016-3.

[49] P.I. Cooper, The absorption of solar radiation in solar stills, Sol. Energy 12 (3) (1969).

[50] Benjamin Y.H. Liu, Richard C. Jordan, The Long-term Average Performance of Flat-Plate Solar-energy Collectors: With Design Data for the U.S., Its Outlying Possessions and Canada, 1963, https://doi.org/10.1016/0038-092X(63)90006-9.